# First-principles mobility prediction for amorphous semiconductors

Yeonghun Lee,[1,2] Yaoqiao Hu,[1] Dongwook Kim,[1] Suman Datta,[3] and Kyeongjae Cho[1,*]
[1]*Department of Materials Science and Engineering, The University of Texas at Dallas, Richardson, Texas 75080, USA*
[2]*Department of Electronics Engineering, Incheon National University, Incheon 22012, Republic of Korea*
[3]*Department of Electrical Engineering, The University of Notre Dame, Notre Dame, Indiana 46556, USA*

(Received 4 January 2022; revised 9 February 2022; accepted 9 February 2022; published 22 February 2022)

Carrier mobility in amorphous semiconductors remained unpredictable due to random electronic states in the absence of the long-range order in a lattice structure, although amorphous semiconductors have been investigated over several decades and widely used in diverse electronic devices. In this work, we develop a method to predict mobility of disordered systems by virtue of the first-principles calculation without using any empirical parameters. Quantum transport modeling based on the nonequilibrium Green's function formalism enables us to establish a formula to connect first-principles results with amorphous-phase mobility. Finally, the developed approach is quantitatively validated by comparing the theoretical predictions with previously measured mobilities of amorphous metal oxides ($SnO_2$, $In_2O_3$, and ZnO) and amorphous silicon. Localization analysis provides further physical insight into a distinct feature between the amorphous metal oxides and amorphous silicon.

DOI: 10.1103/PhysRevB.105.085201

## I. INTRODUCTION

Amorphous and crystalline semiconductors are of interest in various electronic devices for present and future applications: for example, thin-film transistors [1], solar cells [2], phase-change memories [3], organic-electronic devices [4], monolithic three-dimensional integration [5], etc. Electron mobility is a critical figure of merit connected directly to the performance of such devices. To design and optimize semiconductor channel materials, first-principles mobility characterizations have been performed extensively for crystalline semiconductors [6–11]. In line with this, the modeling works have facilitated an accelerated development of electronic device technology by predicting and engineering mobility in a wide range of crystalline semiconductors. On the other hand, the theoretical estimation of mobility for amorphous semiconductors remains elusive due to their disorder-induced complexity in atomic and electronic structures, in which Bloch's theorem is not applicable anymore. Several (semi)empirical and phenomenological models—variable-range hopping [12,13], random phase model [14], Brownian motion model [15], and percolation conduction model [16]—have been presented to explain certain features, such as temperature dependence, of the carrier mobilities in amorphous semiconductors; *ab initio* approaches have been also proposed to model hopping conductions in amorphous semiconductors [17,18]. However, these previous modeling studies have not reached a quantitative description to predict the amorphous-phase mobility that includes both hopping and extended-state conductions without empirical parameters. Given that amorphous semiconductors are ubiquitous and expected to broaden industry applications, it is important to develop a quantitative prediction tool for mobility in amorphous materials based on first-principles calculations without empirical parameters.

In addition to the pragmatic point of view for device applications, conduction in disordered systems exhibits rich fundamental physics problems, such as disorder-induced metal-insulator transition [12,19–21] and many-body localization [22], originating from Anderson localization [19]. Historically, after Anderson localization was suggested in 1958 [19], Thouless introduced an energy scale $E_{\mathrm{Th}} = \hbar D/L^2$ to study the Anderson localization [23–25]. The Thouless energy $E_{\mathrm{Th}}$ corresponds to a coupling strength between levels in two neighboring hypercubes of size $L$ as depicted in Fig. S1 of the Supplemental Material [26], resulting in the energy level broadening. According to the time-energy uncertainty relation, the $E_{\mathrm{Th}}$ is rewritten as $E_{\mathrm{Th}} = \hbar/t$; then, the time $t = L^2/D$ can be interpreted as the escape time for an electron to diffuse escaping out of a block, where $D$ is the diffusion coefficient. Another physical quantity associated with conduction is the average spacing between energy levels, $W$; in a $d$-dimensional hypercube with a density of states $\rho$, $W = 1/(\rho L^d)$. Based on these, Thouless argued that the ratio $E_{\mathrm{Th}}/W$ is proportional to the dimensionless conductance $g = G/(e^2/\hbar) = E_{\mathrm{Th}}/W = (\hbar D/\rho)L^{d-2}$, where $G$ is the conductance. Subsequently, the gang of four—Abrahams, Anderson, Licciardello, and Ramakrishnan—proposed the scaling theory of localization in their influential paper published in 1979 [27]. For weak disorder, Ohm's law holds the validity: $g = \sigma L^{d-2}$, where $\sigma$ is the conductivity. For strong disorder, $g$ decreases exponentially with $L$: $g \propto \exp(-L/\xi)$, where $\xi$ is the localization length. From these two limits, the gang of four asymptotically constructed the scaling function

[*]Corresponding author: kjcho@utdallas.edu

 

$\beta(g) = d \ln g / d \ln L$ and proposed conductivity behavior in disordered systems of different dimensionality. Despite the conceptual success of the scaling theory, quantitative prediction of mobility from scratch remains challenging.

In the present work, we revisit the theory of localization, which provides underlying physical insights into developing a method to quantitatively estimate amorphous semiconductors' mobility in terms of the first principles calculations. More specifically, a universal relationship between mobility and localization length in amorphous phases is established and numerically validated by using a nonequilibrium Green's function (NEGF) method [28–30]. In conjunction with the localization length calculated by the first-principles calculation based on the density functional theory (DFT) [31,32], the relationship established here enables us to not only predict mobility for uncharted amorphous semiconductors but also provide insights into determinant factors of amorphous-phase mobility.

## II. METHODS

### A. NEGF modeling of transport in disordered systems

Quantum transport in disordered electronic systems can be treated by the NEGF method [28–30]. We construct the Hamiltonian $H$, which consists of on-site energies, and hopping parameters for the channel region and self-energies for contacts, in terms of a first-nearest-neighbor $s$-orbital tight-binding model,

$$H = -\sum_i (t_0 \hat{c}_i^\dagger \hat{c}_{i+1} + \text{H.c.}) + \sum_i \varepsilon_i \hat{c}_i^\dagger \hat{c}_i,$$

where $\hat{c}_i^\dagger$ ($\hat{c}_i$) is the creation (annihilation) operator at site $i$, $\varepsilon_i$ is the on-site energy, and H.c. stands for Hermitian conjugate. Amorphous systems are modeled by adding a random on-site energy disorder following a Gaussian distribution with a standard deviation of $\Delta$. Actually, we can adjust either on-site potentials and hopping strengths to model disordered systems because a nonuniform distribution of them results in the same outcome—localization. The hopping parameter $t_0$ is determined by using $t_0 = \hbar^2/(2ma_0^2)$, where $a_0$ is the interatomic distance and $m$ is the effective mass. The elastic phonon scattering is implemented in a phenomenological way using the so-called B$\ddot{u}$ttiker probe model [29,30,33], where the probe extracts electrons and reinjects them after phase randomization. The current at terminal $R$ (or $L$) can be calculated from

$$I_\text{R} = \frac{q}{2\pi\hbar}\int dE\big(\text{Tr}\big[\Sigma_\text{R}^\text{in} A\big] - \text{Tr}[\Gamma_\text{R} G^\text{n}]\big)$$

in terms of an inflow ($\Sigma_\text{R}^\text{in} A$) and an outflow ($\Gamma_\text{R} G^\text{n}$). $q$ is the elementary charge, and $E$ is the energy. Here, $G^\text{n} = G\Sigma^\text{in} G^\dagger$ is the correlation function; $A = i[G - G^\dagger]$ is the spectral function; $\Gamma_\text{R} = i(\Sigma_\text{R} - \Sigma_\text{R}^\dagger)$ is the broadening matrix; $\Sigma^\text{in} = \Sigma_\text{L}^\text{in} + \Sigma_\text{R}^\text{in} + \Sigma_\text{s}^\text{in}$ is the summation of the inscattering functions associated with the two leads and phase-breaking scattering. The retarded Green function $G$ is expressed as

$$G = [EI - H - \Sigma_\text{L} - \Sigma_\text{R} - \Sigma_\text{s}]^{-1},$$

where $\Sigma_\text{L}$, $\Sigma_\text{R}$, and $\Sigma_\text{s}$ are the self-energies, and $I$ is the identity matrix. We calculate the electron current and density based on these approaches, eventually providing mobility in amorphous semiconductors. The $m$ is set to the free electron mass $m_0$, the mean interatomic distance is set to 0.3 nm, and the phonon spectral function $D_0$, which corresponds to the electron-phonon coupling strength, is set to $0.1\,\text{eV}^2$ unless otherwise stated. Temperature $T$ is fixed at 300 K. The intrinsic mobility is calculated within the nondegenerate limit, in which the Fermi level is $3k_\text{B}T$ lower than the conduction band edge. The drain voltage is set to 0.001 V to achieve the low-field limit.

### B. DFT modeling of amorphous semiconductors

The amorphous atomistic structures of $SnO_2$, $In_2O_3$, ZnO, and Si are generated by using *ab initio* molecular dynamics (MD) as implemented in the Vienna Ab-initio Simulation Package (VASP) [34,35]. These calculations were based on DFT using the plane-wave basis set and Perdew-Burke-Ernzerhof generalized gradient approximation (GGA-PBE) functional [36]. The pseudopotential is given by the projector-augmented wave (PAW) method [37,38]. The experimental melt-quench process was simulated to obtain the amorphous atomistic structures [39]. In such a melt-quench method, a supercell of crystalline structure with amorphous-phase densities ($5.29\,\text{g/m}^3$ for $SnO_2$ [40], $6.60\,\text{g/m}^3$ for $In_2O_3$ [41], $5.61\,\text{g/m}^3$ for ZnO [42], and $2.285\,\text{g/m}^3$ for Si [43]) is melt at 3000 K for 6 ps. This step is to remove the crystalline order. The melted supercell is then quenched down to 100 K at a rate of 200 K/ps. We note that this cooling rate is faster than the typical experimental cooling rate of an order of magnitude of 1 K/s, and it is due to the limitation of the time scale in *ab initio* MD simulations. According to a comprehensive experiment-theory work [39], however, the adopted cooling rate is expected to reproduce an experimental atomistic structure well. The obtained quenched structure is finally equilibrated at 300 K for 6 ps, followed by a conventional geometric structure optimization. Since *ab initio* MD is computationally expensive due to the large supercell size and long time scale, we employed a cutoff energy of 250 eV and a single Γ-point Brillouin zone sampling scheme. All simulations were carried out within the $NVT$ ensemble using the Nose-Hoover thermostat [44,45]. The time step was set to 2 fs. For atomistic structural relaxation, the quasi-Newton algorithm method was employed to find a local minimum, with the convergence criterion of the force on each atom to be less than 0.02 eV/Å. Cell shape and cell size were kept constant during the structure relaxation. For electronic minimization and electronic structure calculation, a Blocked-Davidson algorithm was used with the converged energy criterion of $10^{-5}$ eV for total energy.

## III. RESULTS AND DISCUSSION

### A. Relationship between amorphous-phase mobility and localization length

Here, we propose a first-principles mobility modeling for amorphous semiconductors by establishing the universal behavior of mobility. Whereas the original version of the scaling theory of localization was suggested with hypercubes spanning in a three-dimensional (3D) space [27], we focus on the localization length along the transport direction and develop a scaling theory with respect to the channel length in a multichannel one-dimensional (1D) system, which is similar to the approach that has been utilized to develop a different version of scaling theory [46,47] using Landauer's formalism [48]. The multichannel 1D system can correspond to a higher-dimensional system. Apart from that, carrier mobility will be considered rather than conductance because mobility is a directly relevant figure-of-merit to the performance of semiconductor devices.

In accordance with the conductance, the mobility in a noninteracting disordered system relies exponentially on the degree of localization and the characteristic length [20,27,46]:

$$\mu_{\rm amor} = \mu_{\rm cry} \exp\left(-\frac{L}{\xi}\right), \tag{1}$$

where $\mu_{\rm amor}$ and $\mu_{\rm cry}$ are the mobilities in amorphous (with disorder) and crystalline phases (without disorder), respectively. The weak disorder limit gives rise to $\xi \gg L$ and $\mu_{\rm amor} = \mu_{\rm cry}$. A principal parameter constituting the model is the localization length $\xi$, which can also be referred to as a disorder-induced decoherence length. If we assume isotropic delocality of an $L^d$ hypercube, a localization length can be given by

$$\xi_L = L\left(\frac{\rm IPR_{cry}}{\rm IPR_{amor}}\right)^{1/d}, \tag{2}$$

where $\rm IPR_{cry}$ and $\rm IPR_{amor}$ are the inverse participation ratios (IPRs) of crystalline and amorphous phases, respectively. An IPR is a measure of wave-function localization described in $\mathrm{IPR} = (N\sum_i^N |\psi_i|^4)/(\sum_i^N |\psi_i|^2)^2$, where $\psi_i$ is the probability amplitude of an electronic state at the $i$th grid point, and $N$ is the total number of grids. Equation (2) is derived by applying a normalization, $\mathrm{IPR} = \mathrm{IPR_{amor}}/\mathrm{IPR_{cry}}$, which is employed to meet the condition that $\xi_L = L$ for the crystalline system, into the relationship $1/\mathrm{IPR} = (\xi_L/L)^d$. In a 1D $s$-orbital tight-binding model ($d = 1$, $\mathrm{IPR_{cry}} = 1$), Eq. (2) is reduced to $\xi_L = L/\mathrm{IPR_{amor}}$. Importantly, this approach does not end up providing $\xi_L$ larger than $L$ even if the intrinsic localization length $\xi$ is larger than $L$ with a weak disorder. In other words, $\xi_L = L$ ($\xi_L = \xi$) holds when $\xi \gg L$ ($\xi \ll L$). These two opposite limits lead us to expect $1/\xi + 1/L = 1/\xi_L$ or

$$\xi = \left(\frac{1}{\xi_L} - \frac{1}{L}\right)^{-1}, \tag{3}$$

which will be justified later in this work. Equation (3) is highly recommended to use because the first-principles estimation is done with small systems due to computational limitations. Please note that $\rm IPR_{cry}$, $\rm IPR_{amor}$, $\mu_{\rm cry}$, and $\mu_{\rm amor}$ should be averaged under given electron statistics: $\langle A\rangle = \int f(E)A(E)dE/\int f(E)dE$. In tandem with the nondegenerate limit, we adopt the Maxwell-Boltzmann distribution for the $f(E)$. Throughout this paper, we omit the brackets $\langle\cdot\rangle$ for ease of notation. The NEGF modeling turns out to demonstrate that Eq. (1) describes remarkably well the scaling behavior of the mobility regardless of effective masses despite the tenuous form of Eq. (1) [Figs. 1(b) and 1(c)]. Furthermore, this is a piece of evidence that Eq. (3) is valid.

We have so far considered no additional source of level broadening except for the broadening induced by the open boundary condition, i.e., a noninteracting system with contacts at zero temperature. However, additional phase-breaking scattering events (e.g., phonon scattering) are inevitable practically. See Fig. S2 of the Supplemental Material [26] for the effects of disorder and additional phase-breaking scattering on the local density of states (LDOS) and transmission coefficients. In our model, now we introduce electron-phonon coupling with a fixed phonon spectral function $D_0$ using Büttiker probe model [29,30,33] as a source of the incoherent phase-breaking scattering. If other scattering processes are involved, their contributions can be effectively incorporated by adjusting the $D_0$ in Büttiker probe model. Eventually, we establish a relationship for the interacting system by replacing $L$ with $\lambda$ in Eq. (1):

$$\mu_{\rm amor} = \mu_{\rm cry} \exp\left(-\frac{\lambda}{\xi}\right), \tag{4}$$

where $\lambda$ is the mean free path of a crystalline phase. It should be noted that the $\lambda$ in Eq. (4) is a parameter that does not depend on disorder. Actually, in an interacting disordered system, mean free path and localization length are correlated and influenced by each other. However, the interacting, disordered system is divided into an interacting system and a disordered system; then, $\lambda$ and $\xi$ are calculated in each system, which enables us to characterize the mobility of amorphous semiconductors in terms of first principles calculations. This treatment is reasonable because for $\lambda < L$, $\lambda$ play a dominant role of the cutoff characteristic length [20], as schematically shown in Figs. 1(a) and 1(d).

It is necessary to take into account the effects of finite $L$ because a simulation domain for the NEGF modeling cannot be infinitely long. Eq. (4) holds when $L \gg \lambda$; while Eq. (1) holds when $\lambda \gg L$. Connecting these two opposite limits asymptotically, we can derive

$$\mu_{\rm amor} = \mu_{\rm cry} \exp\left(-\frac{L\lambda}{\xi(L+\lambda)}\right). \tag{5}$$

Another effect of the finite $L$ is associated with mobility. Generally, mobility in semiconductors is determined in the long channel limit with a low electric field. When $L$ is comparable to a mean free path, the $L$-dependent mobility emerges. As $L$ decreases, transmission happens more frequently; thus, the transmission coefficient becomes $\lambda/(L+\lambda)$ [49], which will be converted into $\lambda/L$ in the long $L$ limit. Therefore, the ratio of the finite-$L$ transmission coefficient to the infinite-$L$ one is $L/(\lambda + L)$, resulting in

$$\mu_{\rm cry} = \mu_{\rm cry}^{\infty}\frac{L}{\lambda + L}, \tag{6}$$

where $\mu_{\rm cry}^{\infty}$ is the mobility in the long-channel limit. Figure S3 [26] shows that this relationship well describes $\mu_{\rm cry}$ as a function of $L$, so that we exploit Eq. (6) to estimate $\lambda$ in Eq. (5). Also, we further confirmed that $\mu_{\rm amor}$ is $L$-independent for sufficiently large $L$ (Fig. S4 [26]). This $L$-independent $\mu_{\rm amor}$ is required in order for Eq. (4) to hold in the long $L$ limit that we utilize for the first-principles prediction. To numerically validate the model developed for the amorphous-phase mobility prediction, we use Eq. (5) with finite systems, which

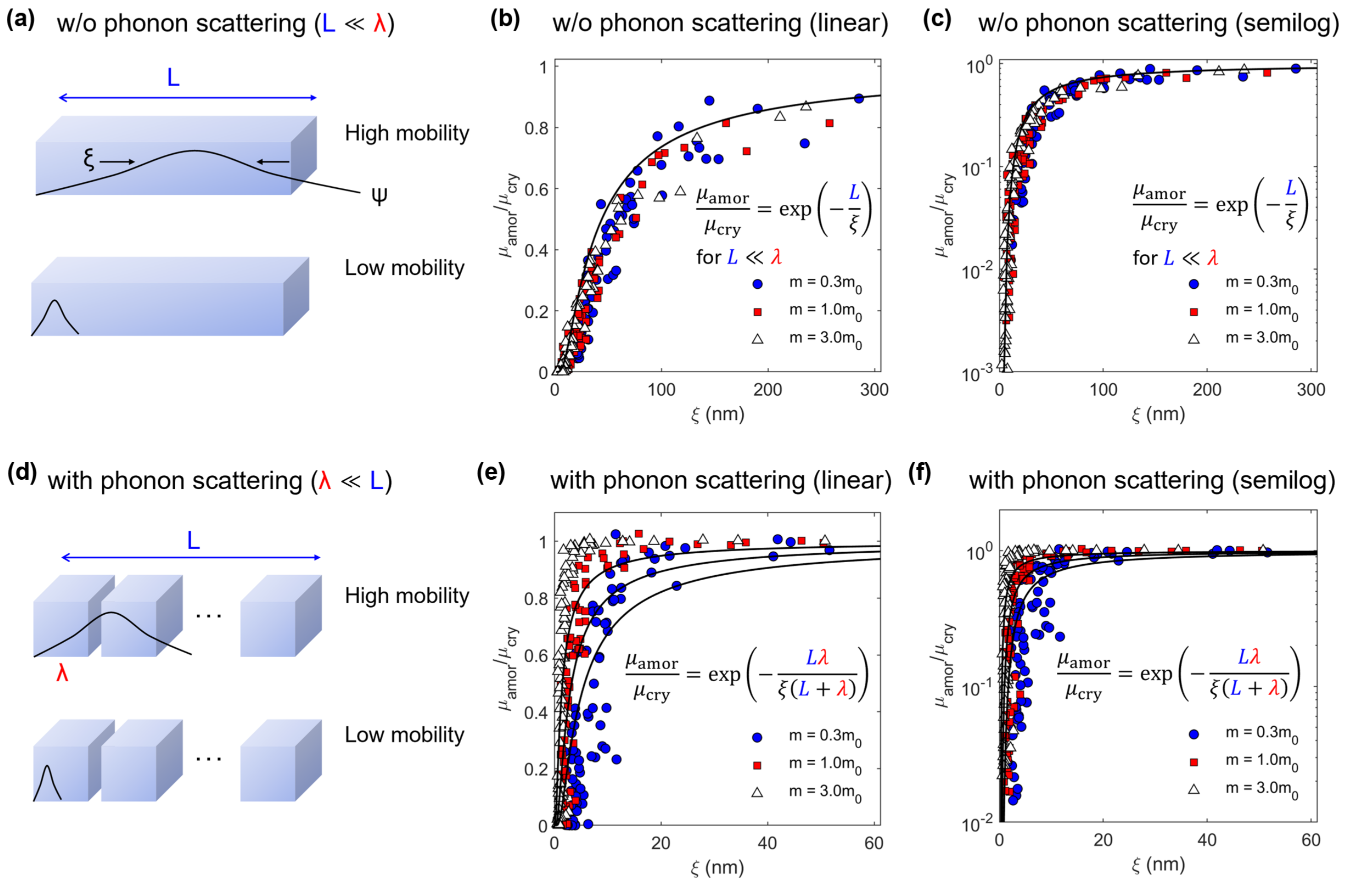


FIG. 1. Relationship between mobility and localization length in 1D systems. (a),(d) Schematics of localization of wave-function envelope $\psi$ in systems (a) without and (d) with phonon scattering. (b),(c) $\mu_{\rm amor}/\mu_{\rm cry}$ as a function of the localization length $\xi$ without phonon scattering [(b) linear, (c) semilog]. (e),(f) $\mu_{\rm amor}/\mu_{\rm cry}$ as a function of $\xi$ with phonon scattering [(e) linear, (f) semilog]. The inset equations are associated with the solid model curves. $L$ is set to 30 nm in (b), (c), (e), and (f).

is still large enough to obtain $L$-independent $\mu_{\rm cry}$ and $\mu_{\rm amor}$. Figures 1(e) and 1(f) show that Eq. (5) reproduces well the overall behavior of $\xi$-dependent mobility with different effective masses. Furthermore, it turns out that the exponential behavior holds as in the noninteracting systems displayed in Figs. 1(b) and 1(c).

### B. First-principles mobility prediction

A combination of the universal relationship and the first-principles calculation can lead to a first-principles amorphous-phase mobility prediction without empirical parameters. Although the current work employs experimental crystalline mobilities to validate the proposed model, they can be replaced with crystalline mobilities simulated by fully *ab initio* apporaches [6–11]. First, we need to make sure that the $\xi$ defined in this work is the intrinsic physical quantity corresponding to the disorder strength of a given amorphous material. In this regard, $\xi$ should be independent of simulation domain size $L$. Figure 2(a) demonstrates that an intrinsic localization length $\xi$ given in Eq. (3) well describes the degree of localization regardless of the system size when the system is sufficiently large. Furthermore, DFT tools dealing with solid states typically exploit periodic boundary conditions of a unit cell. It is necessary to assess the effect of the periodic boundary condition. To do that, we define a localization length in a single unit cell, $\xi_{L,\rm unit} = L_{\rm unit}/{\rm IPR}_{\rm amor}$, where ${\rm IPR}_{\rm amor}$ is calculated in a unit cell in the middle of the system, and $L_{\rm unit}$ is the unit cell size. According to our NEGF calculation, $\xi_{L,\rm unit}$ does not depend on the number of unit cells constituting the entire system but relies only on $L_{\rm unit}$ [Fig. 2(b)]. Also, $\xi_{L,\rm unit}$ is consistent with $\xi_L$ of the fully random system with the same disorder strength [Figs. 2(a) and 2(b)]. In addition, the fitting curve based on Eq. (3) is in good agreement with the numerical results, as shown in Figs. 2(a) and 2(b). These results are pieces of clear evidence that the evaluation of $\xi$ using Eq. (3) along with a periodic boundary condition is valid even if the system is not large enough to show saturation of $\xi_{L,\rm unit}$ with $L_{\rm unit}$.

In the NEGF modeling, we can readily estimate the (phonon) scattering-induced decoherence length $\lambda$ from the size-dependent mobility using Eq. (6), and Fig. S3 [26] shows the fitting works. For the first-principles prediction, however, we need a different solution for $\lambda$ because it is not simple to obtain $\mu_{\rm cry}$ as a function of $L$. Instead, we can utilize the diffusion theory, $\lambda = \sqrt{2D\tau}$, where the two unknowns—diffusion coefficient $D$ and mean free time $\tau$—can be determined by two well-known equations and two readily accessible quantities. By taking the nondegenerate limit, we can take advantage of the Einstein relation $D = \mu_{\rm cry}k_{\rm B}T/q$ to obtain the $D$; also,

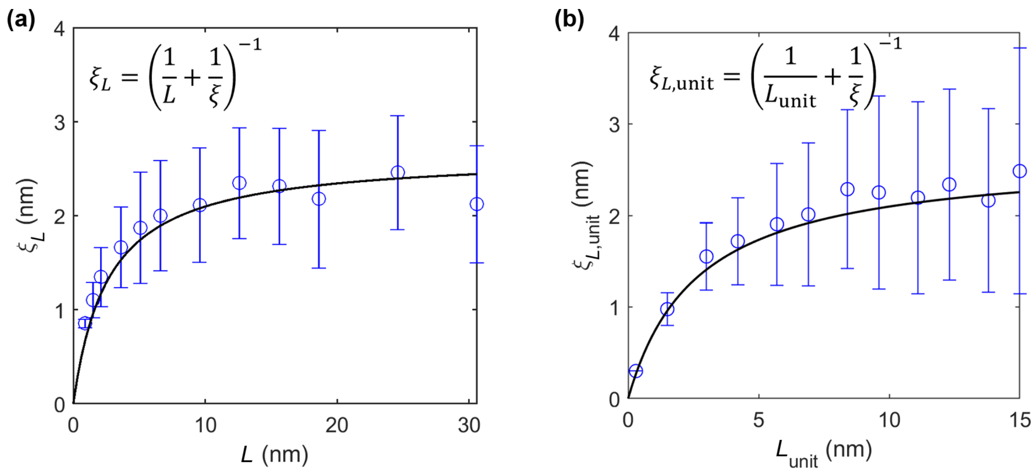


FIG. 2. Validation of the estimation of $\xi$ in 1D systems. (a) Single unit cell localization length $\xi_L$ as a function of $L$ and within fixed disorder strength and without phonon scattering ($\Delta = 0.3\,\mathrm{eV}$, $D_0 = 0\,\mathrm{eV}^2$) using NEGF modeling. Panel (b) shows the same plot but with periodic potential. The system is made of four periodic unit cells with random potential. $L$ is set to 30 nm. The inset equations are associated with the solid fitting curves. The fitting curves in (a) and (b) use the same $\xi$ of 2.65 nm, and each error bar is one standard deviation given by 50 samples randomly generated with the fixed strength of disorder.

the Drude model $\tau = \mu_{\mathrm{cry}} m/q$ enables us to determine the $\tau$. On top of these relations, it will be straightforward to extract the $\mu_{\mathrm{cry}}$ and $m$, either experimentally or theoretically. Putting these equations and parameters together, we derive

$$\lambda = \sqrt{2\mu_{\mathrm{cry}}^2 m k_{\mathrm{B}} T/q^2}, \tag{7}$$

in the end. To calculate the localization length of a 3D system with an arbitrary cell shape, the system size $L$ can be approximated by $L = V^{1/3}$, where $V$ is the cell volume. Finally, we can calculate the mobility of an amorphous semiconductor by combining Eq. (4) and first-principles calculation results.

To validate our model and demonstrate the usefulness of our approach in predicting the mobility in amorphous semiconductors, we apply the mobility model to several selected amorphous solids. The $n$-type metal oxides ($In_2O_3$, $SnO_2$, and ZnO) and Si are chosen as these semiconductors have been widely investigated with their amorphous-phase mobilities experimentally determined. DFT-based first-principles calculations have been performed to generate the amorphous atomic structures and calculate the localization length of the amorphous materials. For each of these materials, multiple amorphous phases (three samples for metal oxides and six samples for Si) have been generated to obtain a statistical average. See Fig. S5 [26] for examples of the calculated electronic DOS and IPR for the selected samples of amorphous materials. In calculating the single unit cell localization length $\xi_{L,\mathrm{unit}}$, IPRs from multiple electronic states are averaged according to the Maxwell-Boltzmann distribution function as we did for the NEGF modeling. The crystalline-phase mobilities are adapted from experimentally reported values [50–53].

The predicted amorphous-phase mobilities in these selected materials, along with their experimentally measured values, are plotted in Fig. 3 (see Table S1 for data of each sample). We note that most of the amorphous Si samples in experiments are passivated by hydrogen to reduce the dangling bond density, including the experimental reference [54], while amorphous Si samples in our model are not hydrogenated. To model the hydrogenated amorphous Si ($a$-Si:H), we mimic the passivation effect by eliminating highly localized states (IPR > 10) that would be originating from the Si dangling bonds [55]. Although very accurate modeling of amorphous phases would be needed for quantitative refinements of the current mobility predictions, Fig. 3 demonstrates that our model can provide a quantitatively reasonable prediction for experimental amorphous-phase mobility reported in articles, especially for the distinct feature between metal oxide systems and Si. Importantly, our model captures the general trend that covalently bonded Si suffers from severer electron mobility degradation than ionically bonded metal oxides when transitioning from crystalline phase to amorphous phase [1]. We can further interpret the inherent difference between metal

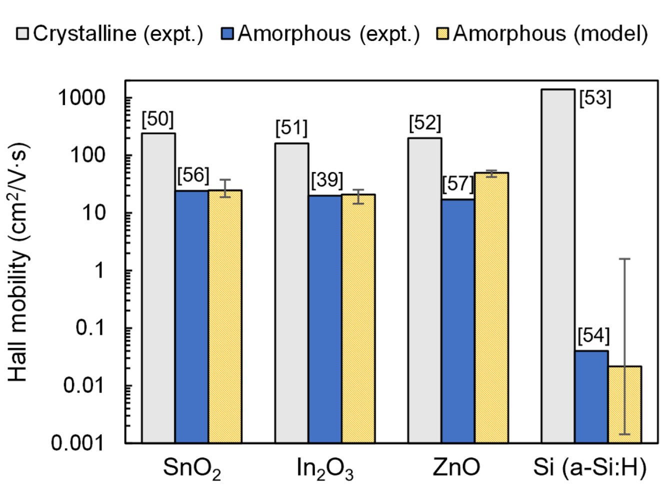


FIG. 3. Amorphous-phase mobilities from experimental Hall measurements [39,54,56,57] and our model. The plot for modeling prediction of the amorphous-phase mobility is an average of logarithmic values with error bars indicating the minimum and maximum values.

oxides and Si by looking into our model analysis. Combining Eqs. (4) and (7), we can obtain $\mu_{\rm amor} \propto \lambda \exp(-\lambda/\xi)$, where $\mu_{\rm amor}$ exhibits a maximum value when $\lambda = \xi$. This relationship indicates that although a large mean free path $\lambda$ provides high mobility of the crystalline phase, a too large $\lambda$ is not desirable to achieve a high $\mu_{\rm amor}$ because $\mu_{\rm amor}$ decreases exponentially when $\lambda$ is larger than $\xi$. This is the case of Si, and the significant degradation of $\mu_{\rm amor}$ is clearly shown from the predicted mobility of amorphous silicon.

## IV. CONCLUSION

We developed and phenomenologically justified a first-principles mobility model for amorphous semiconductors, where the interplay of disorder-induced electron localization and phonon scattering plays a crucial role. Based on the modeling conjunctures, the mobility model quantitatively captures the primary effects of localization on amorphous-phase mobility and reasonably well reproduces the experimentally measured mobilities in amorphous metal oxides and *a*-Si:H. Therefore, the proposed approach is expected to provide quantitative mobility prediction accelerating amorphous materials design for future electronic device applications. While the current work deals with Hall mobility for simplicity, it is worth briefly noting a connection with device mobility. Having considered a high Fermi level, the model here would be applicable to the device mobility even though quantum confinement effects of the inversion layer on electronic states might be challenging to incorporate. Indeed, there is room for improvement in the developed model through careful asymptotic, fine-tuned coefficients, and a rigorous prescription for dimensionality. For all future refinements, this work undoubtedly paves the way for characterizing mobility of amorphous semiconductors, which is accomplished in this work.

## ACKNOWLEDGMENTS

This work was supported by ASCENT, one of six centers in JUMP, a Semiconductor Research Corporation (SRC) program sponsored by DARPA (Grant No. 2018-JU-2776). This work was also supported by the Creative Materials Discovery Program (Grant No. 2015M3D1A1068062) and Nano·Materials Technology Development Program (Grant No. 2016M3A7B4909942) through the National Research Foundation of Korea (NRF) funded by the Ministry of Science and ICT. The authors acknowledge the Texas Advanced Computing Center (TACC) and the National Supercomputing Center (KSC-2021-CRE-0535) for providing supercomputing resources.

[1] K. Nomura, H. Ohta, A. Takagi, T. Kamiya, M. Hirano, and H. Hosono, Room-temperature fabrication of transparent flexible thin-film transistors using amorphous oxide semiconductors, Nature (London) **432**, 488 (2004).

[2] T. D. Lee and A. U. Ebong, A review of thin film solar cell technologies and challenges, Renewable Sustainable Energy Rev. **70**, 1286 (2017).

[3] W. Zhang, R. Mazzarello, M. Wuttig, and E. Ma, Designing crystallization in phase-change materials for universal memory and neuro-inspired computing, Nat. Rev. Mater. **4**, 150 (2019).

[4] N. Nakamura, J. Kim, and H. Hosono, Material design of transparent oxide semiconductors for organic electronics: why do zinc silicate thin films have exceptional properties? Adv. Electron. Mater. **4**, 1700352 (2018).

[5] Y. Son, B. Frost, Y. Zhao, and R. L. Peterson, Monolithic integration of high-voltage thin-film electronics on low-voltage integrated circuits using a solution process, Nat. Electron. **2**, 540 (2019).

[6] T. Gunst, T. Markussen, K. Stokbro, and M. Brandbyge, First-principles method for electron-phonon coupling and electron mobility: Applications to two-dimensional materials, Phys. Rev. B **93**, 035414 (2016).

[7] J.-J. Zhou and M. Bernardi, Ab initio electron mobility and polar phonon scattering in GaAs, Phys. Rev. B **94**, 201201(R) (2016).

[8] Y. Kang, K. Krishnaswamy, H. Peelaers, and C. G. Van de Walle, Fundamental limits on the electron mobility of $\beta$-$Ga_2O_3$, J. Phys.: Condens. Matter **29**, 234001 (2017).

[9] J. Ma, A. S. Nissimagoudar, and W. Li, First-principles study of electron and hole mobilities of Si and GaAs, Phys. Rev. B **97**, 045201 (2018).

[10] Y. Hu, J. Hwang, Y. Lee, P. Conlin, D. G. Schlom, S. Datta, and K. Cho, First principles calculations of intrinsic mobilities in tin-based oxide semiconductors SnO, $SnO_2$, and $Ta_2SnO_6$, J. Appl. Phys. **126**, 185701 (2019).

[11] M. V. Fischetti, P. D. Yoder, M. M. Khatami, G. Gaddemane, and M. L. Van de Put, Hot electrons in Si lose energy mostly to optical phonons: truth or myth? Appl. Phys. Lett. **114**, 222104 (2019).

[12] N. F. Mott, Conduction in glasses containing transition metal ions, J. Non-Cryst. Solids **1**, 1 (1968).

[13] N. F. Mott, Conduction in non-crystalline materials: III. localized states in a pseudogap and near extremities of conduction and valence bands, Philos. Mag. **19**, 835 (1969).

[14] N. K. Hindley, Random phase model of amorphous semiconductors I. transport and optical properties, J. Non-Cryst. Solids **5**, 17 (1970).

[15] M. H. Cohen, Review of the theory of amorphous semiconductors, J. Non-Cryst. Solids **4**, 391 (1970).

[16] T. Kamiya, K. Nomura, and H. Hosono, Electronic structures above mobility edges in crystalline and amorphous In-Ga-Zn-O: percolation conduction examined by analytical model, J. Display Technol. **5**, 462 (2009).

[17] R. Plugaru, T. Sandu, and N. Plugaru, First principles study and variable range hopping conductivity in disordered Al/Ti/Mn-doped ZnO, Results Phys. **2**, 190 (2012).

[18] A. Massé, P. Friederich, F. Symalla, F. Liu, R. Nitsche, R. Coehoorn, W. Wenzel, and P. A. Bobbert, Ab initio charge-carrier mobility model for amorphous molecular semiconductors, Phys. Rev. B **93**, 195209 (2016).

[19] P. W. Anderson, Absence of diffusion in certain random lattices, Phys. Rev. **109**, 1492 (1958).

[20] P. A. Lee and T. V. Ramakrishnan, Disordered electronic systems, Rev. Mod. Phys. **57**, 287 (1985).
[21] M. Imada, A. Fujimori, and Y. Tokura, Metal-insulator transitions, Rev. Mod. Phys. **70**, 1039 (1998).
[22] D. A. Abanin, E. Altman, I. Bloch, and M. Serbyn, Colloquium: many-body localization, thermalization, and entanglement, Rev. Mod. Phys. **91**, 021001 (2019).
[23] J. T. Edwards and D. J. Thouless, Numerical studies of localization in disordered systems, J. Phys. C: Solid State Phys. **5**, 807 (1972).
[24] D. J. Thouless, Electrons in disordered systems and the theory of localization, Phys. Rep. **13**, 93 (1974).
[25] D. J. Thouless, Maximum Metallic Resistance in Thin Wires, Phys. Rev. Lett. **39**, 1167 (1977).
[26] See Supplemental Material at http://link.aps.org/supplemental/10.1103/PhysRevB.105.085201 for a conceptual schematic and additional data.
[27] E. Abrahams, P. W. Anderson, D. C. Licciardello, and T. V. Ramakrishnan, Scaling Theory of Localization: Absence of Quantum Diffusion in Two Dimensions, Phys. Rev. Lett. **42**, 673 (1979).
[28] L. V. Keldysh, Diagram technique for nonequilibrium processes, Zh. Eksp. Teor. Fiz. **47**, 1515 (1964) [Sov. Phys. JETP **20**, 1018 (1965)].
[29] S. Datta, Electrical resistance: An atomistic view, Nanotechnology **15**, S433 (2004).
[30] A. Popescu and P. M. Haney, Effects of phase-breaking scattering on the thermopower of molecular systems, Phys. Rev. B **86**, 155452 (2012).
[31] P. Hohenberg and W. Kohn, Inhomogeneous electron gas, Phys. Rev. **136**, B864 (1964).
[32] W. Kohn and L. J. Sham, Self-consistent equations including exchange and correlation effects, Phys. Rev. **140**, A1133 (1965).
[33] M. Büttiker, Four-Terminal Phase-Coherent Conductance, Phys. Rev. Lett. **57**, 1761 (1986).
[34] G. Kresse and J. Hafner, *Ab initio* molecular dynamics for liquid metals, Phys. Rev. B **47**, 558 (1993).
[35] G. Kresse and J. Furthmüller, Efficient iterative schemes for ab initio total-energy calculations using a plane-wave basis set, Phys. Rev. B **54**, 11169 (1996).
[36] J. P. Perdew, K. Burke, and M. Ernzerhof, Generalized Gradient Approximation Made Simple, Phys. Rev. Lett. **77**, 3865 (1996).
[37] P. E. Blöchl, Projector augmented-wave method, Phys. Rev. B **50**, 17953 (1994).
[38] G. Kresse and D. Joubert, From ultrasoft pseudopotentials to the projector augmented-wave method, Phys. Rev. B **59**, 1758 (1999).
[39] D. B. Buchholz, Q. Ma, D. Alducin, A. Ponce, M. Jose-Yacaman, R. Khanal, J. E. Medvedeva, and R. P. H. Chang, The structure and properties of amorphous indium oxide, Chem. Mater. **26**, 5401 (2014).
[40] C. Avis, Y. Kim, and J. Jang, Amorphous tin oxide applied to solution processed thin-film transistors, Materials **12**, 3341 (2019).
[41] Y. Furubayashi, M. Maehara, and T. Yamamoto, New insights on factors limiting the carrier transport in very thin amorphous sn-doped In2O3 films with high hall mobility, Nanoscale Res. Lett. **14**, 120 (2019).
[42] J. Pilz, A. Perrotta, G. Leising, and A. M. Coclite, ZnO thin films grown by plasma-enhanced atomic layer deposition: Material properties within and outside the atomic layer deposition window, Phys. Status Solidi A **217**, 1900256 (2020).
[43] J. S. Custer, M. O. Thompson, D. C. Jacobson, J. M. Poate, S. Roorda, W. C. Sinke, and F. Spaepen, Density of amorphous Si, Appl. Phys. Lett. **64**, 437 (1994).
[44] S. Nosé, A unified formulation of the constant temperature molecular dynamics methods, J. Chem. Phys. **81**, 511 (1984).
[45] W. G. Hoover, Canonical dynamics: Equilibrium phase-space distributions, Phys. Rev. A **31**, 1695 (1985).
[46] P. W. Anderson, D. J. Thouless, E. Abrahams, and D. S. Fisher, New method for a scaling theory of localization, Phys. Rev. B **22**, 3519 (1980).
[47] P. W. Anderson, New method for scaling theory of localization. II. Multichannel theory of a "wire" and possible extension to higher dimensionality, Phys. Rev. B **23**, 4828 (1981).
[48] R. Landauer, Electrical resistance of disordered one-dimensional lattices, Philos. Mag. **21**, 863 (1970).
[49] M. Lundstrom and Z. Ren, Essential physics of carrier transport in nanoscale MOSFETs, IEEE Trans. Electron Devices **49**, 133 (2002).
[50] Z. M. Jarzebski and J. P. Marton, Physical properties of $SnO_2$ materials: II. Electrical properties, J. Electrochem. Soc. **123**, 299C (1976).
[51] R. L. Weiher, Electrical properties of single crystals of indium oxide, J. Appl. Phys. **33**, 2834 (1962).
[52] D. P. Norton, Y. W. Heo, M. P. Ivill, K. Ip, S. J. Pearton, M. F. Chisholm, and T. Steiner, ZnO: Growth, doping & processing, Mater. Today **7**, 34 (2004).
[53] S. Nashima, O. Morikawa, K. Takata, and M. Hangyo, Measurement of optical properties of highly doped silicon by terahertz time domain reflection spectroscopy, Appl. Phys. Lett. **79**, 3923 (2001).
[54] E. K. Sichel, L. Greber, and K. Wang, Hall effect in amorphous Si:H and amorphous Si:H/amorphous Ge:H superlattices, Appl. Phys. Lett. **52**, 1074 (1988).
[55] M. Legesse, M. Nolan, and G. Fagas, Revisiting the dependence of the optical and mobility gaps of hydrogenated amorphous silicon on hydrogen concentration, J. Phys. Chem. C **117**, 23956 (2013).
[56] J. H. Ko, I. H. Kim, D. Kim, K. S. Lee, T. S. Lee, B. Cheong, and W. M. Kim, Transparent and conducting Zn-Sn-O thin films prepared by combinatorial approach, Appl. Surf. Sci. **253**, 7398 (2007).
[57] K. Nomura, A. Takagi, T. Kamiya, H. Ohta, M. Hirano, and H. Hosono, Amorphous oxide semiconductors for high-performance flexible thin-film transistors, Jpn. J. Appl. Phys. **45**, 4303 (2006).